JOURNAL OF SPACECRAFT AND ROCKETS
Vol. 46, No. 4, July–August 2009

Postflight Analysis of Inflatable Reentry and Descent Technology Blackout During Earth Reentry

Philippe Reynier*
Ingénierie et Systèmes Avancés, 33702 Mérignac, France
and
David Evans†
Fluid Gravity Engineering, St. Andrews, Fife, Scotland KY16 9NX, United Kingdom

DOI: 10.2514/1.41480

The Inflatable Reentry and Descent Technology flight performed in 2006 was not nominal. The flight was characterized by a blackout period shorter than expected. Here, we apply two methods that can be used to perform postflight analysis. The first, based on an engineering approach, has already been used for the preflight analysis. The second involves coupled calculations between a computational fluid dynamics and an electromagnetic solver. The main objective of this postflight analysis is to validate this advanced approach using flight data and to assess the validity of the engineering method. Numerical results show that the engineering method overpredicts the blackout duration due to the fact that this method is based on a severe on/off switch. The coupled approach leads to an underestimation of the blackout period. Several uncertainties, such as the influence of ablative material on ionization, could explain this discrepancy. Analysis establishes the validity of the coupled approach, but its accuracy depends strongly on the modeling used for the calculations.

Nomenclature

E_z	=	Z component of the electric field in the direction of Earth, V/m
F_{np}	=	Fourier transform without plasma
F_p	=	Fourier transform in the presence of plasma
f_{link}	=	link frequency, Hz
f_p	=	plasma frequency, Hz
m_e	=	electron mass, kg
n_e	=	electron number density, m^{-3}
$n_{e,\text{crit}}$	=	critical electron number density, m^{-3}
q	=	electron charge, C
t	=	time from launch, s
ε_0	=	permittivity of vacuum, F/m

I. Introduction

IN THE frame of the Manned Spaceflight and Exploration Programme and of the Technological Research Programme of the European Space Agency, several Earth entry orbital demonstrators were developed. Among them, three Inflatable Reentry and Descent Technology (IRDT) demonstrators [1] were developed in cooperation with the European Aeronautic Defence and Space Company and the Babakin Space Center (BSC) in Russia and flown from 2000 to 2005.

The use of an inflatable technology has some impact for the entry analysis. If the inflatable structure is used as a backward-braking device, the same phenomenon can occur as it does for flows around flaps. As for a flap, the presence of a backward device can induce some local heating due to the presence of gaps and/or corners, and the flowfield itself can be influenced by strong fluid/structure interactions [2]. The main aspect of the inflatable technology is at the system level; indeed, the use of an inflatable device is much more complex than the choice of a rigid heat shield. Inflation of the device occurs at high altitude and high velocity, and this presents a key problem in the absence of a ground-test facility capable of reproducing this process of in-flight conditions.

The last vehicle of the IRDT series, IRDT-2R or Demonstrator-2R, was launched successfully on 7 October 2005. However, an incident occurred during the flight, most probably due to the bursting of the inflatable device, inducing a nonnominal trajectory and resulting in the loss of the capsule, which was not recovered. IRDT-2R was equipped with an autonomous radio telemetry system (ARTS) antenna operating at a frequency of 219 MHz, embedded in the front shield, to ensure communications during the flight except during the blackout period. From the data recovered before the end of transmission from the capsule, the blackout period was also found to be nonnominal.

This paper focuses on the analysis of the blackout duration during the IRDT-2R flight. From the nonnominal trajectory rebuilt at the European Space Research and Technology Centre (ESTEC), based on the scenario of a deflation of the main inflatable breaking device (MIBD) during the flight, an analysis of the blackout duration has been undertaken using engineering and advanced approaches. The engineering method, already used for the mission preparation [3], is based on shock-layer analysis and correlations of critical electron number density with transmission frequency. The advanced approach makes use of a coupling between computational fluid dynamics (CFD) and electromagnetic simulations.

II. Trajectory Analysis

This section describes the mission and in-flight scenarios. The analysis performed at ESA-ESTEC [4] and the trajectory retained for the blackout analysis are briefly reviewed.

A. Nominal Scenario

The nominal scenario of the IRDT mission is shown in Fig. 1. The mission can be summarized as follows. The launch was performed from a Russian submarine in the Barents Sea by a Volna rocket. After the separation of the capsule and its spin-off, the entry occurred at a 100 km altitude with an entry velocity of 6869 m/s and took place at 60.88-deg-lat north and 159.2-deg-long. east. The reentry angle was −6.84 deg. The inflatable device consists of (see Fig. 1) two parts: the MIDB and the additional inflatable breaking device (AIBD). MIBD

Presented as Paper 3894 at the 39th AIAA Plasmadynamics and Lasers Conference, Seattle, WA, 23–26 June 2008; received 8 October 2008; revision received 6 February 2009; accepted for publication 3 February 2009.

*Research Engineer, B.P. 20005, 19 Allée James Watt; Philippe.Reynier@isaspace.eu.

†Senior Scientist, 83 Market Street; David.Evans@fluidgravity.co.uk.

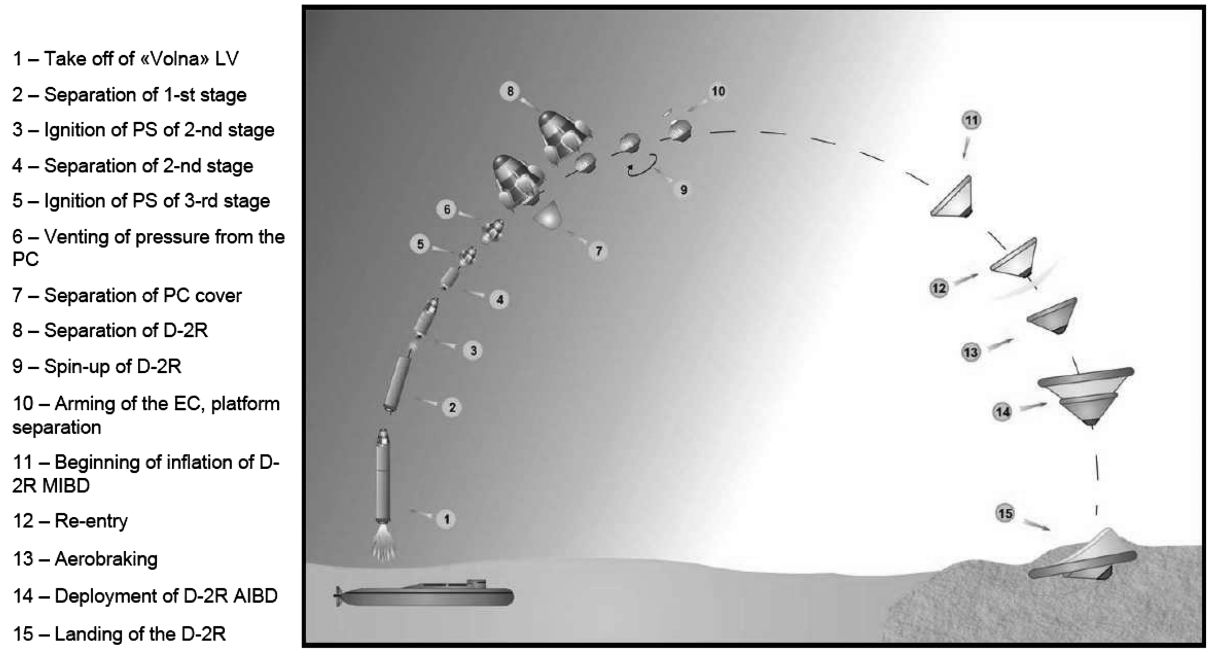

Fig. 1 Nominal mission profile of IRDT-2R (credit to Babakin Space Center) [16]. Abbreviations used are LV for launch vehicle, PS for propulsion system, PC for payload compartment, *D-2R* for demonstrator 2R, EC for experiment compartment, MIBD for main inflatable braking device, and AIBD for additional inflatable braking device.

deployment was planned to be achieved just before the reentry, and AIBD deployment occurred at a nominal value of 7.5 km. The landing was planned in the Kamchatka Peninsula.

During the mission, communications with the ground were ensured through a telemetry antenna system, ARTS, operating in the very-high-frequency (VHF) band with a frequency of 219 MHz. In the mission scenario, the blackout zone was planned to start at the beginning of the reentry at 100 km of altitude and $t = 906.94$ s (from launch) and it was to end at $t = 986.94$ s, and so the duration was 80 s. The blackout duration estimated at the BSC was 60 s, but with a margin of 20 s, and hence the duration of the mission plan [5].

B. In-Flight Scenario

The in-flight scenario, summarized in Fig. 2, was different from what was expected. The launch was successful, as was the separation of the capsule from the cover, the spin-off, and the inflation just before reentry at $t = 906.38$ s. The flight was nominal until the beginning of the blackout zone, starting a little later than expected, at $t = 923.695$ s from launch. Thus, the blackout duration was shorter than expected, with a duration of 45.338 s. The telemetry was lost at $t = 992.41$ s, and at the time of writing, the capsule had not been recovered.

The analysis of the flight data shows that the gravitational-load evolution during the flight was not nominal. The gravitational-load distributions computed at BSC and ESTEC for a nominal flight are compared with the flight data in Fig. 3. There is a slight difference between the trajectory calculated at ESTEC and BSC, with a maximum of gravitational load predicted 4 s earlier than in the BSC's trajectory. This discrepancy might be due to some differences in the atmosphere models used in the calculations. The flight data are in good agreement with the nominal predictions before the blackout. However, a huge discrepancy is clearly evident after the end of the blackout period, which shows that, if the trajectory was nominal before the blackout period, this was not the case after the end of the blackout.

C. Recovery of Flight Trajectory

A trajectory analysis has been carried out at ESTEC [4] with the objective of finding a reliable interpretation of the flight data. According to this study, the most reliable explanation for the nonnominal trajectory is the deflation of the MIBD during the reentry. This is highlighted in Fig. 4, in which the gravitational-load distributions computed for different scenarios (MIBD fully deflated, almost completely deflated, and half-deflated) are plotted. The different characteristics such as the base diameter and the reference area used to compute the trajectory are reported in Table 1. The scenario in which the MIBD is almost completely deflated at $t = 55$ s (from the beginning of reentry at 100 km of altitude) provides the best fit to the flight data. Other postflight trajectory analysis carried out at Institute für RaumfhartSysteme [6] and BSC [7] arrived at the same conclusions. As a consequence, this scenario, based on the hypothesis of an almost complete deflation of the MIBD during reentry, has been retained as the baseline for the current study on blackout.

III. Engineering Approach for Blackout Analysis

A high level of electron density around the spacecraft during the flight increases the attenuation and can lead to the blackout phenomenon associated with ionization. When a critical density of electrons for a given frequency is reached, communication is no longer possible. The critical electron densities for the different communication bands [8] (VHF, S, X, and Ka) are listed in Table 2. During the IRDT flight, the communications with the ground were effected by the ARTS. The ARTS antenna was operating in the VHF band at a frequency of 219 MHz. The antenna, embedded in the heat shield as shown in Fig. 5, had an annular shape (with the stagnation point as center) and was emitting in the forward direction [5]. This means that the signal emitted by the antenna had to cross the shock wave located upstream of the vehicle front shield. During entry, ARTS was not to be used during the blackout period, and so for mission planning, the duration of the blackout period had to be estimated.

To complete the postflight analysis based on trajectory predictions, a study has been undertaken to reassess previous blackout predictions during the flight as a function of the new trajectory. This has been carried out in two steps. In the first step, an engineering approach developed and used already for the mission preparation [3] has been applied to the postulated flight trajectory. In the second step, a more advanced method based on coupled simulations between CFD and electromagnetic solvers has been developed.

A. Engineering Method

During a reentry, a high level of electron density around the spacecraft can lead to the communications blackout that is associated

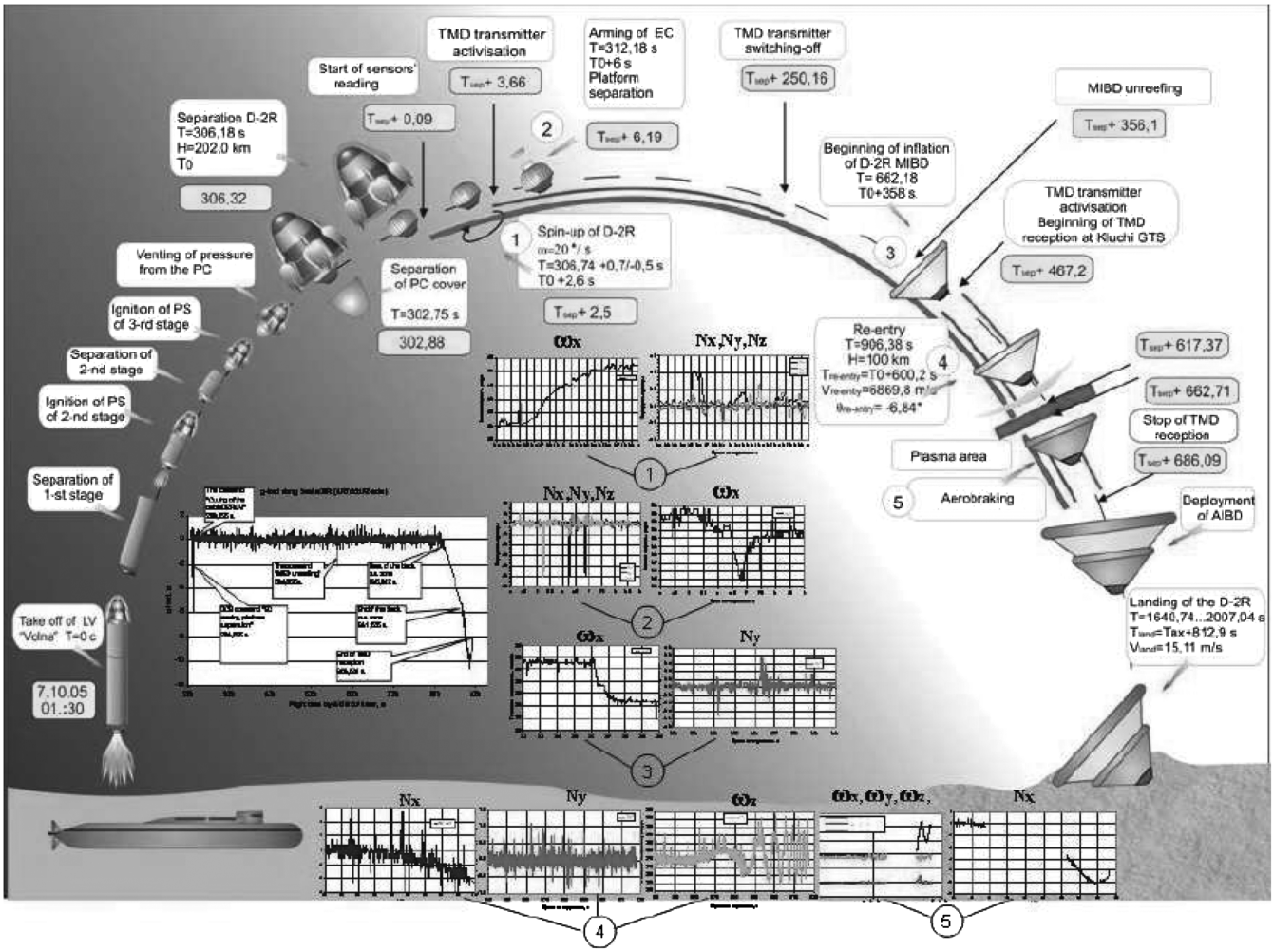

Fig. 2 Flight mission profile of IRDT-2R mission (credit to Lavochkin Association) [7].

with ionization. For a preliminary analysis, an in-depth study of the blackout coupled to three-dimensional numerical simulations of the IRDT configuration at different locations during the early stages of the reentry could not be undertaken. Therefore, an engineering approach was developed to predict the blackout duration.

This method, based on an on/off switch, is described here. Phenomena such as diffraction, coupling with radiation, and propagation of electromagnetic waves within the plasma are beyond the scope of this engineering study and are not addressed here. Signal attenuation is also not considered here. To assess the blackout duration, the critical electron density for the ARTS frequency has to be determined. When the critical density of electrons is reached, it is assumed that the communication link is cut. For a given electron density n_e, the corresponding plasma frequency f_p in hertz is expressed as

$$f_p = \frac{1}{2\pi}\sqrt{\frac{q^2 n_e}{\varepsilon_0 m_e}} \tag{1}$$

where q is the electron charge, m_e is the electron mass, and ε_0 is the permittivity of vacuum. From this equation, the critical density $n_{e,\mathrm{crit}}$ for a communication band is given as

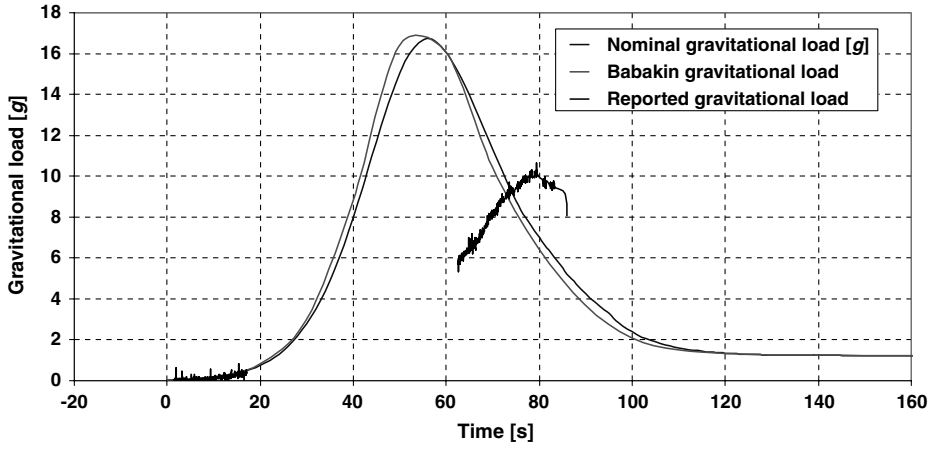

Fig. 3 Gravitational-load distributions computed at ESTEC (nominal gravitational load) and BSC for the nominal trajectory and flight data (reported gravitational load) [4].

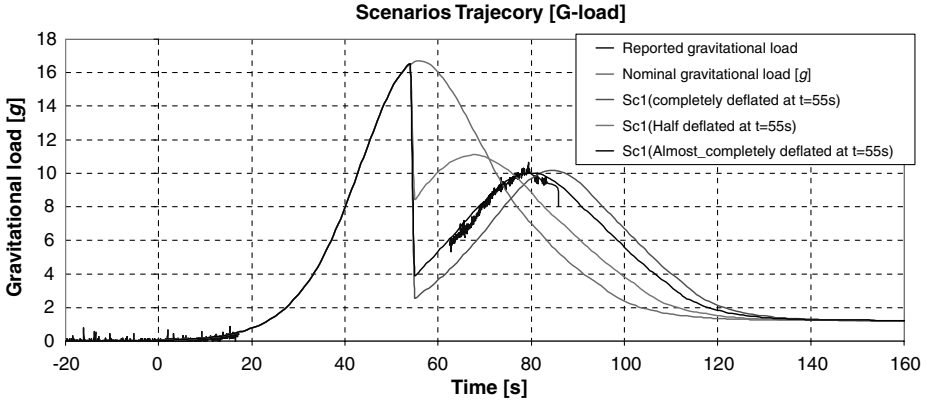

Fig. 4 Gravitational-load distributions and sensitivity analysis for the deflation scenario.

$$n_{e,\text{crit}} = \frac{f_{\text{link}}^2}{80.64 \times 10^6} \tag{2}$$

where f_{link} is the link frequency, expressed in hertz. Applying this equation to the ARTS frequency of 219 MHz, the critical density for this antenna is found to be 0.594×10^9 electrons per cubic centimeter.

To predict the electron number density around the thermal protection system (TPS), the chemistry composition along the stagnation line has been computed using the shock-layer solver PMSSR [9] for different points on the trajectory. Using this tool, an axisymmetric approach is used to determine the composition of the shock layer accounting for chemical and thermal nonequilibrium. Here, an Earth atmosphere thermochemical model [10] accounting for ionization, with 11 species (N_2, N_2^+, N, N^+, O_2, O_2^+, O, O^+, NO, NO^+, and e^-) and 16 chemical reactions have been used for the calculations. According to Greendyke et al. [11], only minor differences can be found between axisymmetric and three-dimensional computations for blackout prediction. In this work, only one thermochemical model is used, whereas a parametric study [11] has shown a particular sensitivity of the onset and severity of electron-avalanche phenomena associated with changes in the thermochemical model. An extension of this study would be to perform a parametric study of the chemistry composition with several thermochemical models.

Using this methodology, the electron number density is computed with PMSSR along the stagnation line and compared with the critical electron number densities at the link frequency. This can be used as a first estimate of the blackout duration, because the antenna is located close to the stagnation point.

B. Preflight Analysis

Using this methodology to prepare for the mission [3], the electron number density was computed and compared with the critical densities for the ARTS and the other frequency bands reported to provide predictions of the mission blackout duration.

Several computations have been made for different times of IRDT entry, from $t = 906.94$ to 971.94 s. The calculations have been stopped when the electron density was lower than the critical density for the ARTS frequency. The electron density has been computed along the stagnation line, because the antenna is embedded in the front shield. The electron density at the antenna location and at the stagnation point should be of the same order, but may vary more significantly with the antenna look angle. In Fig. 6, the electron number densities, based on PMSSR estimates, are computed for different points of the trajectory and plotted along with the critical electron densities for different bands. Results show that the critical electron number density for the Ka band is reached at $t = 966.94$ s, which corresponds to the peak of heat flux during the entry. It is also the moment with the highest ionization effects. The predicted blackout duration lasts only a few seconds in this band. The blackout duration for X and S bands are close to 35 and 50 s, respectively. For the frequency of interest here, the ARTS frequency, the blackout duration is longer. According to our numerical results, it lasts 60 s.

The blackout duration during the IRDT mission has also been estimated at BSC [5]. According to this work, the blackout zone lasts from the start of reentry at $t = 906.94$ to 986.94 s. This was longer than the predictions with, at first sight, a discrepancy of 20 s. However, for the mission preparation, a margin of 20 s was considered for the entry beginning, and this margin was included in the blackout duration prediction. This explains the apparent discrepancy between the blackout duration considered for the mission design and the predictions performed with the engineering method. The blackout duration estimated by BSC, before the addition of the 20 s margin, was 60 s, and so this is in very good agreement with the predictions performed at ESTEC.

C. Postflight Analysis

To estimate the reliability of the engineering approach developed for the mission analysis, it is of interest to apply it in the postflight analysis. This has been done during the reentry from $t = 0$ to 80 s for the trajectory corresponding to the scenario with an almost completely deflated MIBD shown in Fig. 4. From the trajectory derived using the flight data, the electron number densities along the stagnation line have been computed and compared with the critical density for the ARTS band. Figure 7 shows the flight data with the gravitational-load distribution, the electronic density computed at the stagnation point, and the critical electronic density for the ARTS band. The beginning and end of the blackout period are also reported in Fig. 7. During the flight, the blackout period lasted from $t = 17.315$ to 62.65 s from the reentry time, thus lasting 45.3 s, which is less than predicted during the mission preparation.

The beginning of the entry is nominal and, as for the mission preparation, the computations predict the beginning of the blackout zone at $t = 7$ s after reentry. The blackout zone is expected to last until $t = 75$ s: therefore, 12.4 s after the end of the blackout zone

Table 1 Configuration of the capsule selected for different scenarios [4]

	MIBD completely deflated	MIBD half-deflated	MIBD almost completely deflated
Nose radius, m	0.61	0.61	0.61
Base diameter, m	0.89	1.6	1.1
Reference area, m^2	0.622	2.04	0.95
Mass, kg	130	130	130

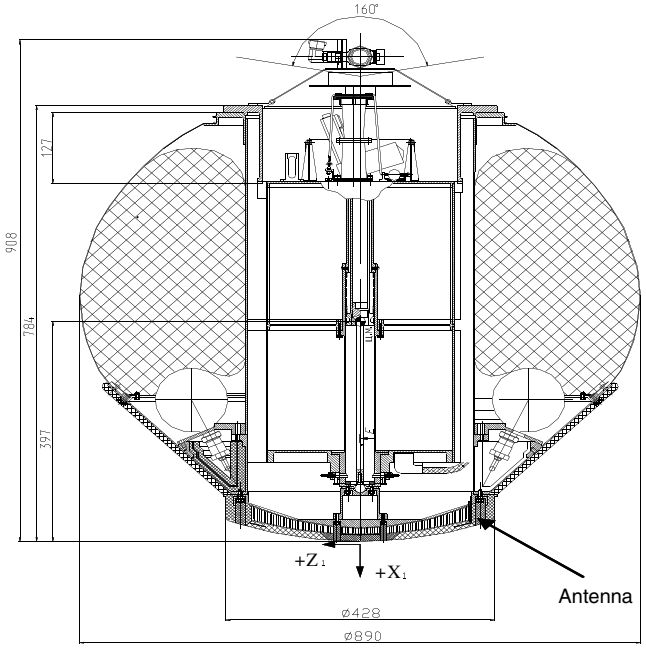

Fig. 5 Sketch of IRDT with embedded antenna location.

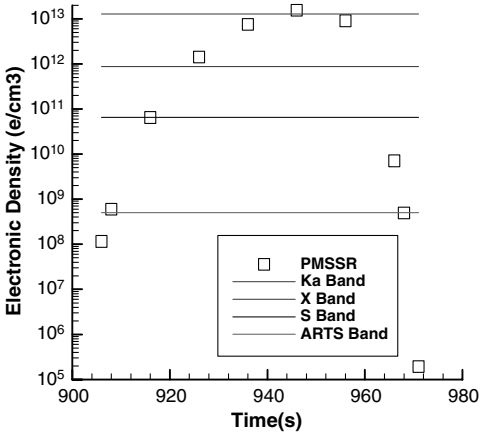

Fig. 6 Evolution of the electronic density during IRDT entry. The lines correspond to the critical density for Ka, X, S, and ARTS bands.

during the flight. Thus, the engineering method predicts the onset of blackout 10.3 s earlier and the end 12.4 s later than the flight data. The duration of the blackout zone is overpredicted by 22.7 s: a blackout duration of 45.3 s during the flight compared with 68 s in our computations.

The discrepancy between the predictions and the flight data can be explained by several factors. A previous study [11] has established a particular sensitivity to the onset and severity of an electron-avalanche phenomenon associated with changes in the thermochemical model. Such a fact could explain the discrepancy in the onset of the blackout period but not the discrepancy at the end of the blackout period. Another point is the approach itself that might be too elementary to handle such a phenomenon. Indeed, this engineering method is a rather severe on/off switch, not accounting for partial attenuation signal-to-noise ratios. An extension of this study could include a parametric study of the chemistry composition with several thermochemical models. A possibility to refine the approach would be to use electron densities predicted by CFD computations. The present analysis also neglects the ablation process that could create species increasing or decreasing the level of ionization in the shock layer. To provide a better assessment of the blackout period, in the next section, coupled calculations will be performed using CFD and electromagnetic solvers.

IV. Coupled Approach

To refine the results obtained using the engineering approach and also to assess its reliability, a coupled approach has been applied to the problem. This blackout analysis is based on the coupling between the numerical simulations performed using TINA [12], which are postprocessed using a suite of codes. The method is described hereafter.

A. CFD Predictions

During a reentry, the high level of electron density around the spacecraft induces the signal attenuation or blackout that is associated with ionization; as a consequence, the numerical simulations performed with TINA have been performed accounting for this phenomenon. For this objective, the thermochemical model proposed by Park [10] has been retained. This is an 11-species model (O_2, N_2, O_2^+, N_2^+, O, O^+, N, N^+, NO, NO^+, and e^-) with 16 chemical reactions. Computations have been performed without surface catalysis; because the maximum of the electron population is close to the shock location, their mass fraction at this location should not be modified by catalytic boundary conditions.

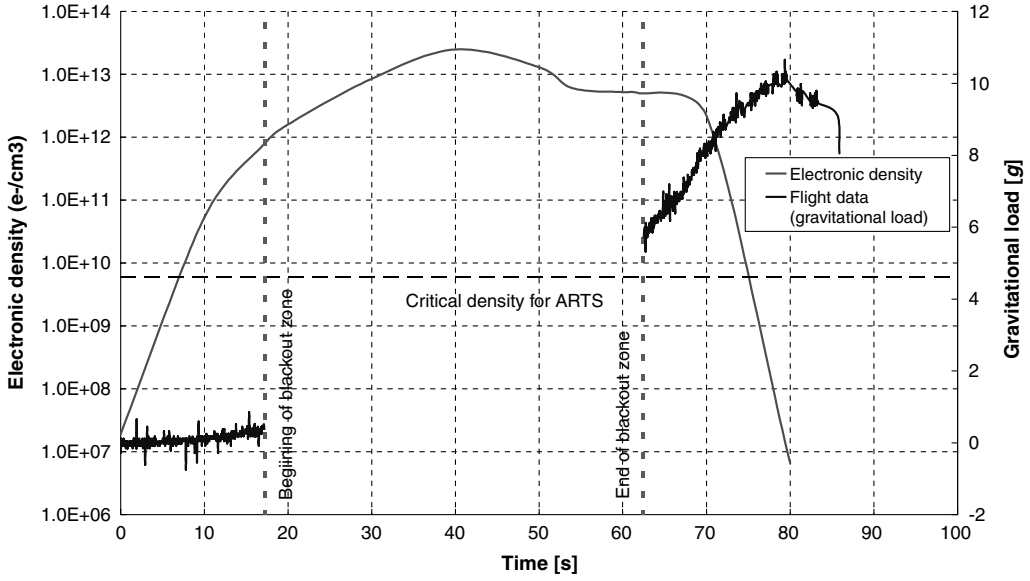

Fig. 7 Evolution of the electronic density during IRDT entry and flight data for the g load. The horizontal line corresponds to the critical electronic density for the ARTS band.

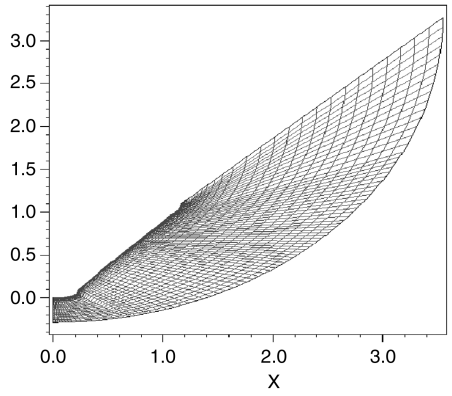

Fig. 8 Mesh used for the computations.

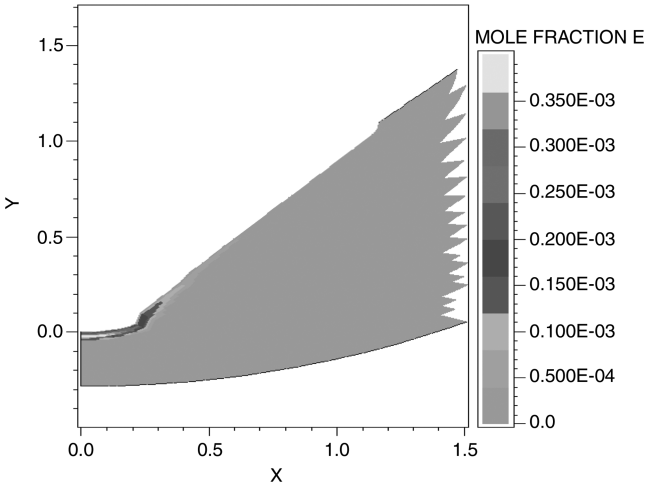

Fig. 9 Mole fraction of electrons at peak heat flux of the nominal trajectory.

Axisymmetric computations have been performed assuming a 0 deg angle of attack for the capsule. During the flight there was a nonzero angle of attack that has been neglected here. The axisymmetric mesh used for the calculations is an 85×50 cell mesh and is plotted in Fig. 8.

Numerical predictions have been performed for the trajectory points reported in Table 3. First, computations have been carried out for the point of the nominal trajectory corresponding to peak heating conditions (43 s). This point lies in the strongest part of the blackout region and this calculation is used to test the suite of codes. Then numerical simulations have been performed for the start (17 s) and end (62 s) points of the blackout region observed during the flight.

A TINA prediction is shown in Fig. 9, in which the mole fraction of electrons is plotted, and the corresponding mass fraction is shown in Fig. 10. This solution was obtained for the trajectory point corresponding to the maximum of heat flux along the nominal IRDT trajectory [13].

Computations have been performed using some modifications in the calculation of the ambipolar diffusion. The lower limit for this quantity has been reduced from 10^{-9} to 10^{-19}. This modification of the ambipolar diffusion assumption for small electron number densities has been performed to avoid a high (erroneous) electron density in the freestream. The calculations were also performed with a very low level of the inflow mass fraction of electrons: 10^{-20}. If a very low mass fraction is not used at the inflow, this may result in an overestimation of the electron number density in the whole field.

The predictions for the two other trajectory points of Table 3 have been achieved assuming the same computational conditions.

B. Methodology

First, the results from TINA (2-D mesh, electron mass fraction, electron temperature, and electron number density) are mapped to a 3-D orthogonal mesh using the link code FLING [14]. The 3-D mesh used in FLING includes the entire reentry vehicle. It spans 180 cells along the x and z directions and 108 cells along the y direction; the domain extends from -3 to 3 m in the x and y directions and from -1 to 2.6 m in the y direction.

The same tool computes the electron collision frequency and the plasma frequency in each cell of the mesh. Then the Maxwell equations are used to solve the electric field corresponding to ARTS transmission through the plasma flow using the electromagnetic solver PLASMA [14].

In PLASMA's input, the antenna location and characteristics have to be provided. Here, the antenna has been located in the cell as close as possible to the real configuration shown in Fig. 5. Because the PLASMA code works in the time domain, it is more convenient to use a broadband Gaussian pulse instead of the 219 MHz sinusoidal waveforms, because they do not provide very good results.

For assessment of the blackout duration during reentry, the PLASMA output case to be postprocessed is the one corresponding to the far field, which corresponds to what is seen by the receiver on Earth. The prediction of E_z (electric field in the z direction) is sufficient. To estimate the blackout, the following approach has been adopted. First, the electric field at the antenna has to be generated from the vehicle nose. This is done by driving a current in a cell near the antenna. Next, the code PLASMA has to be run again, but without plasma. This gives an unattenuated signal that we can use to calculate the attenuation.

Figure 11 shows the signals seen by the receiver on Earth for the plasma-case and no-plasma-case runs. The signal is a derivative of the Gaussian pulse having been transmitted through what is, in effect, a dipole antenna. The attenuation is easily seen as the differences

Table 2 Minimum frequencies and critical electronic densities for different communication bands. Note that the Ka band here is the deep space band not the near-Earth band.

Link frequency, GHz	Designation	Critical electronic density, electrons/cm^3
0.219	vhf band	5.94×10^8
2.3	S band	6.56×10^{10}
8.4	X band	8.75×10^{11}
32.0	Ka band	1.27×10^{13}

Table 3 Characteristics of the trajectory points investigated

Trajectory	Time from reentry, s	Atmospheric relative velocity, m/s	Altitude, km	Atmospheric free density, kg/m^3
Nominal	43	5800	66	2×10^{-4}
Flight	17	6860	85.8	7.23×10^{-6}
Flight	63	3355	50.6	8×10^{-4}

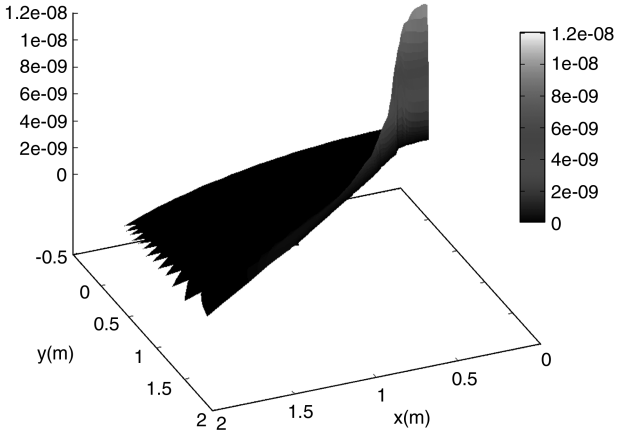

Fig. 10 Electron mass fraction at peak heat flux at 43 s (nominal trajectory case).

between those two curves. There is a second small signal seen at the end of the run. This is due to a reflection off the back of the computational mesh that is not physical and can be ignored.

The last step is to estimate the attenuation for the receiver on Earth measured in decibels. For this, both outputs from PLASMA are postprocessed using a discrete Fourier transformation. After the Fourier transform is completed, the last 10 ns of data from the file are removed, because they include only the physically meaningless reflection from the PLASMA mesh boundary. The minimum and maximum frequencies required for the calculations using the discrete Fourier transformation tool [14] have been set to 10 and 1000 MHz.

The results obtained after the Fourier transformation is performed, with and without the plasma, are plotted in Fig. 12. This figure shows a strong attenuation of the signal due to the plasma.

The final step is to calculate the attenuation itself. The results shown in Fig. 12 are then converted to the loss of the signal power in decibels, as described hereafter.

If F_p is the Fourier transform of the plasma case and F_{np} is the Fourier transform of the no-plasma case, both in amplitude units, then the attenuation (att) in decibels is given by

$$\text{att} = 20 \log \frac{F_p}{F_{\text{np}}} \tag{3}$$

The results displayed in Fig. 13 show a plasma attenuation of about 9 dB expected at the ARTS radio link frequency. A dish antenna of the type that might be used on the ground and used at low frequencies ($\sim$1 GHz) typically has a gain of around 15 dB. Hence, this loss of 9 dB might not be enough to explain the loss of communications, because there could still be some net gain in the communications link. There is, however, an issue with the mesh dependence of the results. Usually, one wavelength should be spanned by 8 to 10 cells. Here, the wavelength for the frequency of 219 MHz is 0.73 m, which means that the mesh should be sufficient because the cells are 3.33 cm per side. However, the plasma zone is only 10 cm wide, and so this is covered by only 3 cells. This might lead to significant loss of information on the shock plasma.

Therefore, other runs have been carried out by using a reduced domain extending in the x and y directions from -1.8 to 1.8 m with 108 cells and from -0.5 m to 1.8 m in the y direction with 69 cells. Next, a more refined mesh has been used on the same domain with 360 cells in the x and z directions and 230 along the y direction. With this last mesh, the cells are spaced only 1 cm apart.

The attenuations calculated for the different meshes are plotted in Fig. 14. There is little difference between the two first meshes, because the cell sizes are not very different. The reduction in coverage of the PLAMSA mesh does not seem to affect the results in any significant way. Thus, we can concentrate on just the nose section of the vehicle and use a higher-resolution mesh. With the high-resolution mesh, the attenuation computed is around 14 dB. This loss of 14 dB almost cancels out the gain of the receiving antenna, and so this is likely to be enough to lose communication. However, more information on the communications link is necessary to confirm this result.

To assess the blackout duration during IRDT reentry, this coupled method has been applied and calculations have been performed for the trajectory points corresponding to the beginning and the end of the blackout zone (see Table 3).

C. Blackout Duration Estimation

Numerical simulations of the flowfields around the IRDT capsule have been carried out for the beginning and end trajectory points of the blackout region. The numerical results have been coupled to the Maxwell solver using the high-resolution mesh. The signal attenuation as a function of frequency for the beginning point of the blackout period is shown in Fig. 15. The attenuation computed for the beginning point at the ARTS frequency is 17 dB, which is high

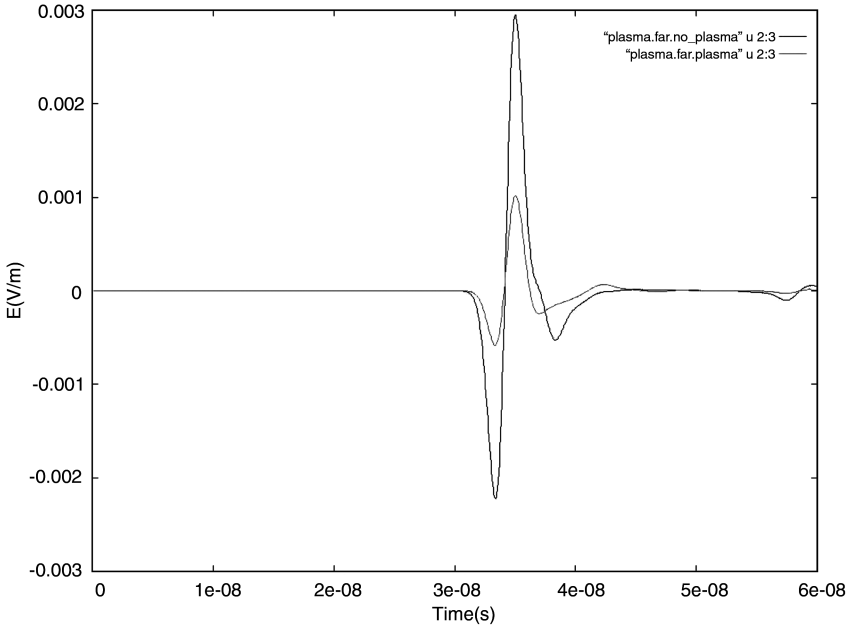

Fig. 11 Signals received on Earth with (small amplitude) and without (large amplitude) plasma attenuation.

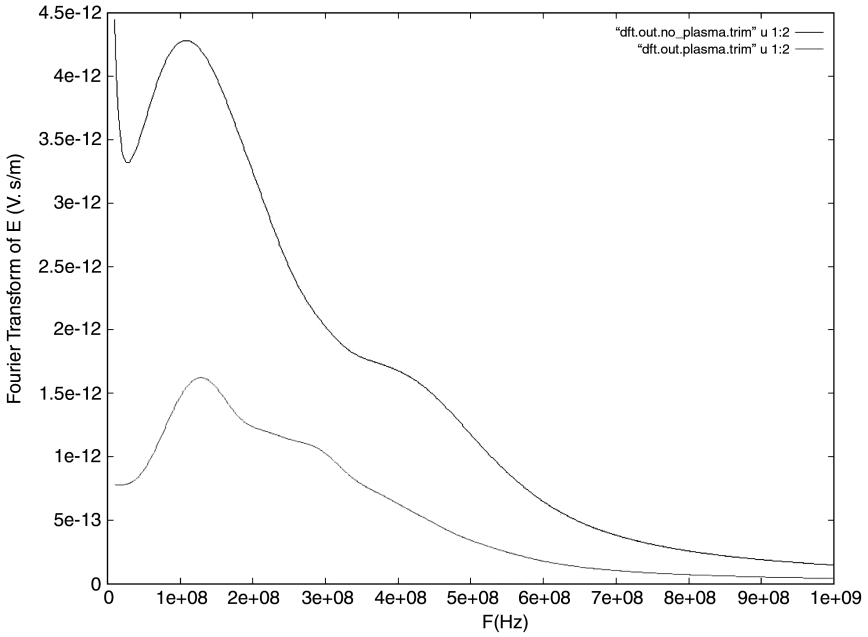

Fig. 12 Fourier transforms of the calculations with (bottom line) and without (top line) plasma as a function of the frequency.

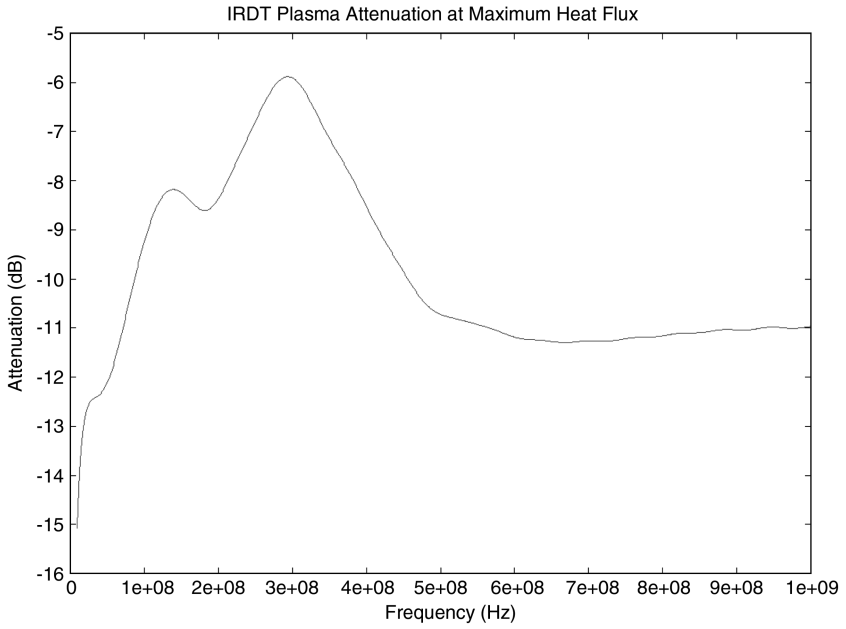

Fig. 13 IRDT plasma attenuation in decibels as a function of the frequency.

enough to fit with the beginning of the blackout zone observed during the flight if we consider a critical value of 15 dB for a dish antenna with a frequency lower than 1 GHz. Moreover, the onset of blackout is very rapid, due to the phenomenon of electron avalanche at the beginning of entry when the capsule enters in the first layers of the atmosphere.

The attenuation computed for the end point is plotted in Fig. 16. The attenuation is around 12 dB at the link frequency of 219 MHz. This level seems to be a little bit low, but because the radio link frequency is much lower than 1 GHz, this level of attenuation might be sufficient to predict the end of the blackout region. More accurate predictions would require additional knowledge of the communications link budget. This is difficult because there is little information available on this point.

Now let consider the critical values for the transmission to the ground station. During reentry, IRDT is tracked by the Lyzyk ground station [16]. According to the Babakin Space Center [16], the ground station can receive the spacecraft signal when its strength is higher than -118.8 dB. The signal strength received by the station for the period corresponding to the beginning to the end of the blackout zone ranges from -95 to -93 dB. The calculated attenuation is -17 dB at the beginning and -12 dB at the end. Adding these attenuation figures to the preceding numbers, we get values of -112 dB at the beginning and -105 dB at the end. Comparing with the station sensitivity of -118.8 dB, this should still be detectable at the ground station. The information provided [16] is only provided for a few points along the trajectory and is only valid for the nominal trajectory. There may be some variability between the points given and the actual sensitivity for the end point of the blackout zone.

Overall, the effects of the plasma are suspected to be underestimated in this study. The method is sound but depends critically on obtaining the correct estimate of the electron density. This means using a more optimal mesh around the vehicle and including any effects that may change the predicted ionization level, such as the chemistry model or the effects of ablation.

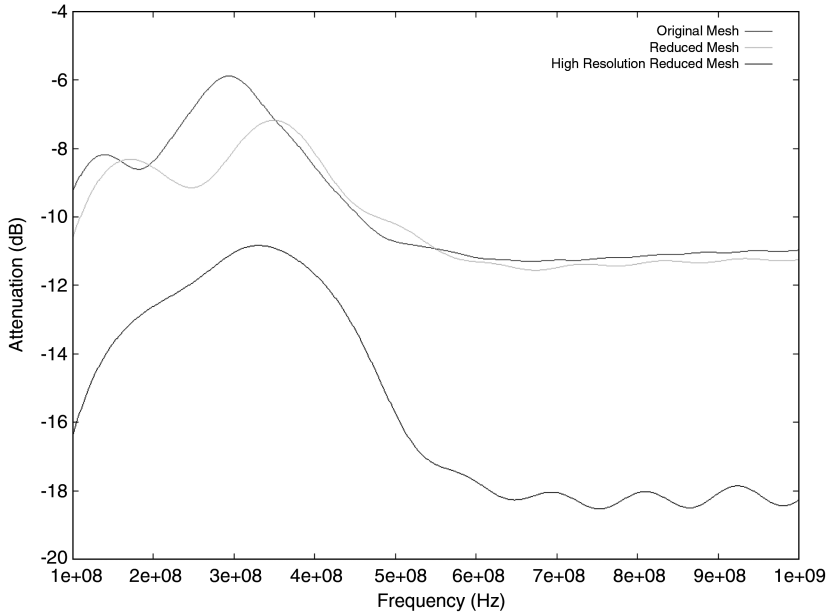

Fig. 14 Attenuation predictions obtained with the original, the reduced, and the high-resolution reduced meshes.

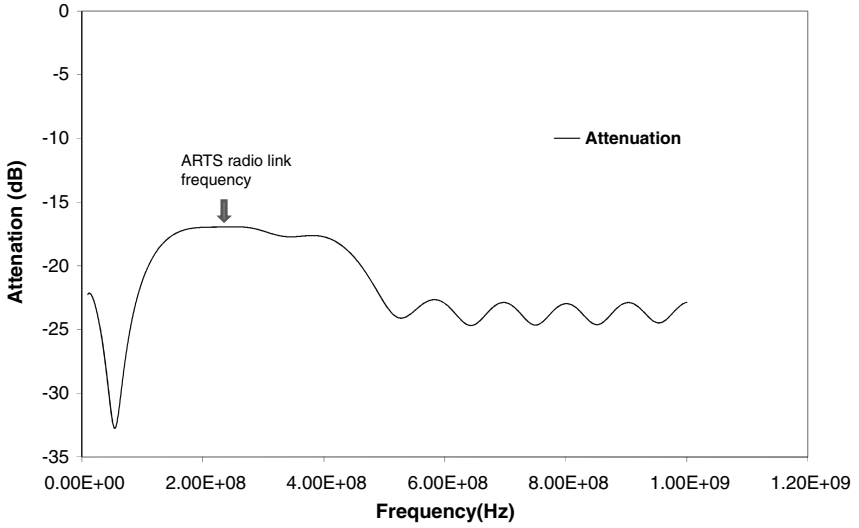

Fig. 15 Plasma attenuation computed for the beginning point of the blackout region.

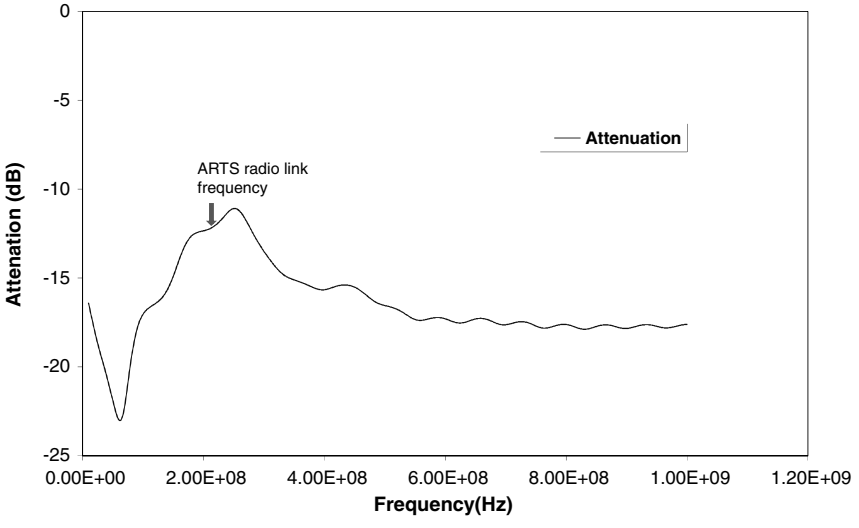

Fig. 16 Plasma attenuation computed for the end point of the blackout region.

This last point is important, because the injection of material species in the shock layer, such as sodium that is used in the fabrication process of some TPS materials [15], can significantly increase the electron density. Moreover, due to the lack of flight or experimental data on ionization in the available literature, it is even difficult to give an estimate on the uncertainty on the predictions on the electron number density.

V. Conclusions

A postflight analysis of the blackout duration of the IRDT reentry has been carried out. First, an engineering method already applied for the mission preparation has been used. This approach is based on a shock-layer prediction tool coupled to the critical link frequency for the electron density. This approach has been able to predict a blackout region, including the one observed during the flight.

Then a coupled approach between CFD and electromagnetic solvers has been developed and applied to the postflight analysis. Computations have been performed for the beginning and end points of the blackout region. The results show a lower level of attenuation than necessary for the ground station sensibility. The agreement seems to be acceptable for the beginning point, but the station should still be able to receive the signal from the spacecraft at the end.

The two methods studied both have problems. The engineering model assumes a one-dimensional shock and probably overestimates the electron density. The application of this to determine transmission is basically an on/off switch, which is a rather severe assumption. The coupled CFD approach needs a lot of care to ensure that all the important physical features are accurately modeled: optimized mesh, high resolution, and chemistry model, including all ionization factors. The ablation products from the TPS pyrolysis are not considered in this study. Depending on the TPS composition and blowing efficiency in the shock layer, these products might have a strong influence on the shock-layer composition and therefore on the electron density. This phenomenon could, by itself, explain some of the differences between the attenuation predicted and the observation making use of what is known about the critical sensitivity of the ground station. The usefulness of the two methods has been demonstrated in this study, but their accuracy is still a subject for further study.

Acknowledgments

This work has been supported by ESA through contract 16666 CCN4/2006. The authors of this paper would like to thank Arthur Smith from Fluid Gravity Engineering and Lionel Marraffa from ESA's European Space Research and Technology Centre for their valuable advice and suggestions.

References

[1] Marraffa, L., Kassing, D., Baglioni, P., Wilde, D., Walther, S., Pitchkhadze, K., and Finchenko, V., "Inflatable Re-Entry Technologies: Flight Demonstration and Future Prospects," *ESA Bulletin*, Vol. 103, Aug. 2000, pp. 78–85.

[2] Mack, A., and Schäfer, R., "Fluid Structure Interaction on a Generic Body-Flap Model in Hypersonic Flow," *Journal of Spacecraft and Rockets*, Vol. 42, No. 5, 2005, pp. 769–779. doi:10.2514/1.13001

[3] Reynier, P., and Marraffa, L., "Aerothermodynamics Investigations for Earth Orbital Entry Vehicles," 4th International Symposium on Atmospheric Reentry Vehicles and Systems, Association Aéronautique et Astronautique de France, Paper 32_79, Mar. 2005.

[4] Boutamine, D. E., Marraffa, L., Mazoué, F., and Reynier, P., "IRDT Trajectory: Reconstruction of Flight Data," ESA, European Space Research and Technology Centre, Noordwijk, The Netherlands, Nov. 2005.

[5] "IRDT-2RE-Flight Mission: Design Defination Report," Babakin Space Center, Rept. BSC-IRDT2R-DDR-0004_Rev4, Moscow, Feb. 2005.

[6] Gräßlin, M. H., "IRDT-2R Reentry Trajectory Post Flight Evaluation," Inst. für Raumfhart Systeme, Univ. of Stuttgart, Stuttgart, Germany, Feb. 2006.

[7] "IRDT-2R: Final Presentation," Lavochkin Association, Moscow, and and Babakin Space Center, Moscow, Feb. 2006.

[8] Morabito, D. D., "The Spacecraft Communications Blackout Problem Encountered During Passage or Entry of Planetary Atmospheres," California Inst. of Technology, Jet Propulsion Lab., Interplanetary Network Progress Rept. 42-150, Pasadena, CA, 2003.

[9] Dubois, J., and Smith, A. J., "Program PMSSR V4.1: Inverse Shock Layer Solution with Nonequilibrium Thermochemistry," TN 132/92-Issue 3, Fluid Gravity Engineering, Emsworth, England, U.K., Aug. 2004.

[10] Park, C., "Review of Chemical-Kinetic Problems of Future NASA Missions, 1: Earth Entries," *Journal of Thermophysics and Heat Transfer*, Vol. 7, No. 3, 1993, pp. 385–398. doi:10.2514/3.431

[11] Greendyke, R. B., Gnoffo, P. A., and Lawrence, R. W., "Calculated Electron Number Density Profiles for the Aeroassist Flight Experiment," *Journal of Spacecraft and Rockets*, Vol. 29, No. 5, 1992, pp. 621–626. doi:10.2514/3.11501

[12] TINA, Software Package, Ver. 4, Fluid Gravity Engineering, Emsworth, England, U.K., Jan. 2007.

[13] "IRDT-2RE-Flight Mission: Summary Analysis Report," Babakin Space Center, Rept. BSC-IRDT2R-SAR-0001, Moscow, Nov. 2003.

[14] Reynier, P., and Evans, D., "PLASMA-FLING User Manual," Ingénierie et Systèmes Avancés, TN 01V2-2007, Mérignac, France, July 2007.

[15] Jenniskens, P., Wercinski, P., Olejniczak, J., Allen, G., Desai, P. N., Raiche, G., Kontinos, D., Revelle, D., Hatton, J., Baker, R. L., Russell, R. W., Taylor, M., and Rietmeijer, F., "Preparing for Hyperseed MAC: An Observing Campaign to Monitor the Entry of the Genesis Sample Return Capsule," *Earth, Moon, and Planets*, Vol. 95, Nos. 1–4, 2004, pp. 339–360.

[16] "IRDT-2RE-Flight Mission: Design Definition Report," Babakin Space Center, Rept. BSC-IRDT2R-SAR-0004, Moscow, Feb. 2005.

I. Boyd
Associate Editor